The Fracture Performance of Basalt Fiber-reinforced Autoclaved Aerated Concrete

Wenli Quan[1], Wei Huang[1*], Wenbo Sun[2], and Peng Zhang[3]

[1] School of Civil Engineering, Xi'an University of Architecture & Technology, Xi'an, 710055, China

[2] Xi'an University of Architecture & Technology of South Australia An De College, Xi'an, 710055, China

[3] China Railway Xi'an Group CO.LTD, Xi'an, 710000, China

1775999076@qq.com

Abstract: The basalt fiber-reinforced autoclaved aerated concrete (BF/AAC) specimens were prepared and the corresponding fracture performance were investigated in this study. The relationship curve of load and displacement were obtained and then the crack initiation load and ultimate load were determined. Then the fracture toughness calculated according to double-K fracture model and the fracture energy were calculated. The results show that as the basalt fiber (BF) content grows, the bending degree of macro crack path on the fracture surface increases slightly, while the fracture toughness and the fracture energy increase to varying degrees. When the BF content is 0.4%, the specimen shows the best fracture performance, and the corresponding initiation toughness, fracture toughness, and fracture energy increase by 43.34%, 86.66%, and 117.75%, respectively. In addition, the microscopic morphology of BF/AAC sample was observed. The SEM results show that BF can bridge micro crack in AAC matrix.

Keywords: Autoclaved aerated concrete, Basalt fiber, Fracture toughness.

1 Introduction

With the repaid development of civil engineering technology in recently years, more and more new cementitious materials have been applied in buildings, such as engineering cementitious composite (ECC), lightweight concrete, etc. Among them, the combination of lightweight concrete and prefabricated components can significantly reduce the weight of prefabricated concrete component and structure, which not only reduces the economic costs of transportation and lifting, but also helps to reduces the seismic response of building structure effectively. On the other hand, due to that the crack propagation is a common problem in concrete structures during service, which effects the stability and durability of structures, the analysis of the fracture performance of structural materials to seek methods for controlling the cracks propagation in structure has become one of the current research hotspots. Therefore, it

W. Guo et al. (eds.), *Proceedings of the 3rd International Conference on Green Building, Civil Engineering and Smart City (GBCESC 2024)*, Advances in Engineering Research 264,
https://doi.org/10.2991/978-94-6463-728-1_40

is necessary to conduct research on the fracture performance of the new material before it is applied in structural component.

Autoclaved aerated concrete (AAC) is a lightweight silicate product. The bulk density and thermal conductivity of AAC are only 1/4 and 1/10 of ordinary concrete, respectively. Therefore, AAC products have been widely applied in buildings. In order to fully utilize the lightweight advantages of AAC, some scholars have combined AAC with structural components and proposed some new composite prefabricated floor slabs and walls. Huang et al.[1] proposed a prefabricated composite wall formed by AAC infilled blocks and concrete ribbed columns and beams. Under seismic loads, AAC blocks fail and consume some energy, which can serve as the first defense line against earthquakes in the wall. Y. Yardim et al.[2] developed a lightweight composite floor slab made of AAC concrete filled with AAC blocks, which is well enough to give warning before failure. Zhang et al. and Xu et al[3] also proposed a lightweight composite floor slab composed of reinforced AAC bottom plate and post pouring concrete. Under the same size, the weight of this lightweight slab reduced by 20% to 30% compared to that of ordinary concrete slabs.

Although the high porosity made AAC lightweight, the mechanical strength and crack resistance are relatively poor. Up to now, there have been some researches on improving the basic mechanical performances of AAC by using different fibers, such as carbon fiber (CF), basalt fiber (BF), polypropene fiber (PF), glass fiber (GF), kaoline fiber (KF), and plant fiber[4]. However, Li[5] pointed out that some fibers may not be suitable for enhancing AAC. CF is relatively expensive and significantly increases the thermal conductivity of AAC. The melt point of PF (170℃) is lower than that of the autoclaved temperature (usually 180~190℃), therefore, PF may be destroyed and damage the pore wall of AAC during the production process. KF would be corroded severely in alkaline AAC slurry. The improvement effect of GF on the AAC is poor. Plant fibers are not easily dispersed in AAC slurry. Therefore, considering the fiber price, alkali resistance, and their impact on the pore structure and thermal conductivity of AAC, BF is more suitable for industrial production of AAC. In addition, AAC are mainly used in non-structural parts of buildings at present, studies on the performance of fiber-reinforced AAC (FAAC) only involved the basic physical and mechanical properties, such as dry density, compressive strength, and thermal conductivity. Although there have been a few reports on the fracture properties of AAC by early researchers such as Feng [6], the fracture properties of FAAC have never been investigated.

Refer to the literatures [4] and take into account the prices of different fibers, BF is selected to enhance AAC in this investigation. The fracture performance of BF-reinforced AAC (BF/AAC) with different fiber content will be studied through three-point bending beam tests with cracks. Moreover, the micro morphology of BF/AAC samples will be observed.

2 Experimental Program

2.1 Specimen preparation

The grade of BF/AAC is B06A3.5. All the raw materials, including tailing sand, cement with P · O42.5 grade, quicklime, gypsum, foaming agent, and BF, were provided by Hanzhong Derun Environmental Protection Technology Co., Ltd. The length and diameter of BF were 3mm and 7-15μm, respectively.

Take in to account of fiber content of 0, 0.1%, 0.2%, 0.3%, 0.4%, and 0.5%, a total of six sets of specimens were designed. Each group contains three notched beam specimens with size of 100mm × 100mm × 400mm. The information of prefabricated crack was shown in Fig. 1.

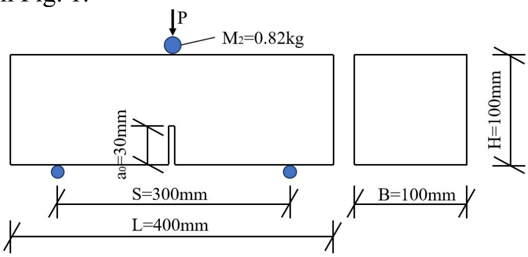

Fig. 1. Information of notched BF/AAC beam specimens

2.2 Test methods

A pair of aluminum plates were attached on the bottom surface specimen with crack, and then an electronic extensometer (YC10/4 type) was installed to measure the crack mouth opening displacement (CMOD) at the bottom of prefabricated crack at any time. The loading rate was 0.6 mm/min, with a displacement control mode. After the specimens was damaged, the micro morphology was observed through electron scanning microscope (SEM) test.

3 Experimental results

3.1 Micro morphology and failure mode

The final failure phenomena of BF/AAC specimens and the micro morphology of BF/AAC-0.4 sample were shown in Figs. 2 and 3, respectively. Fig. 2 indicated the fracture surfaces of all specimens were located at the mid span position, and the bending degree of the macro crack paths on the fracture surface showed a slight increase trend with the fiber content increased. In Figs. 3(a)~(b), BF bridged the microcracks in AAC matrix, and the adhesion between BF and pore wall matrix was good. Under the external load, the deformation of BF and the frictional interaction between BF and AAC matrix consumed some energy, which to some extent changed the crack path. However, BF itself belonged to siliceous materials. During the autoclaved curing process, BF participated into the CaO-SiO_2-H_2O hydrothermal reaction with calcareous materials, which resulted in fiber corrosion[4] (Figs. 3(c)~(d)). Therefore, the effect of BF on constraining cracks was limited.

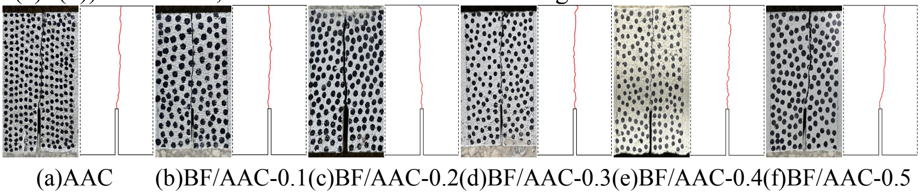

Fig. 2. Failure mode of BF/AAC

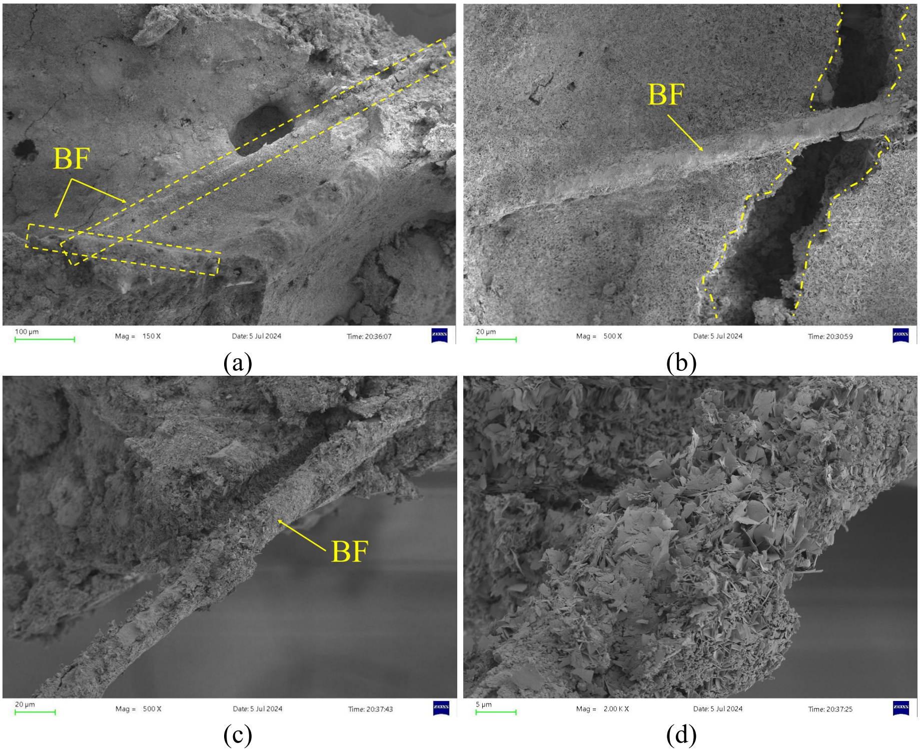

Fig. 3. Microscopic morphology of BF/AAC-0.4

3.2 Fracture performance

Crack initiation load and ultimate load. The crack initiation load (P_{ini}) and ultimate load (P_{max}) can be obtained from the $\boldsymbol{P-\varepsilon}$ curve and $\boldsymbol{P-COMD}$ curve, respectively, as shown in Fig. 4. Moreover, the brittleness of the BF/AAC specimens can be characterized through the ratio of P_{ini} to P_{max}. Table 1 showed the P_{ini}, P_{max}, and the P_{ini}/P_{max} values of BF/AAC specimen with different BF content.

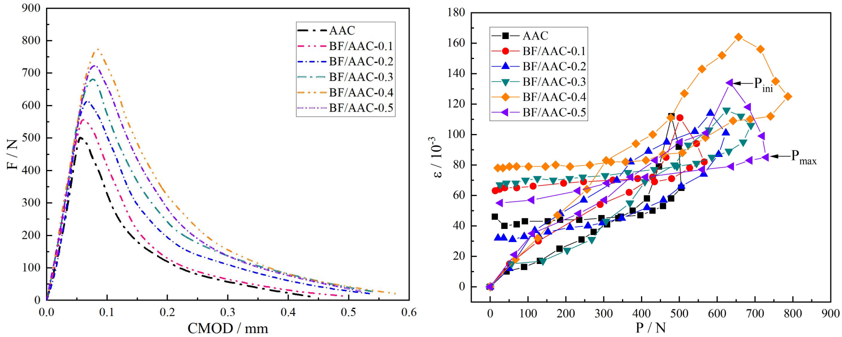

(a) $\boldsymbol{P-COMD}$ curve (b) $\boldsymbol{P-\varepsilon}$ curve

Fig. 4. $P-COMD$ curve and $P-\varepsilon$ curve of BF/AAC

Table 1. P_{ini} and P_{max} of BF/AAC

No.	P_{ini} (N)	P_{max} (N)	P_{ini}/P_{max}
AAC	471	505	0.933
BF/AAC-0.1	510	566	0.901
BF/AAC-0.2	560	623	0.899
BF/AAC-0.3	613	689	0.890
BF/AAC-0.4	675	789	0.858
BF/AAC-0.5	631	729	0.866

It can be seen from Table 1 that the P_{ini} and P_{max} both showed an upward and then downward tendency. Whereas, the P_{ini}/P_{max} showed an opposite trend. When the BF content was 0.1%, 0.2%, 0.3%, 0.4%, and 0.5%, respectively, the P_{ini} increased 8.28%, 18.39%, 30.15%, 43.31%, and 33.97%, respectively, while the P_{max} increased 12.08%, 23.37%, 36.44%, 56.24%, and 44.36%, respectively. The P_{ini} and P_{max} both reached their maximum at the fiber content of 0.4%. The values of the P_{ini}/P_{max} showed that BF improves the fracture resistance and brittleness of AAC. This was because BF bridged the microcracks in AAC matrix, which improved the crack resistance and ultimate bearing capacity of AAC. However, when the fiber content exceeded 0.4%, BF might be unevenly distributed in the AAC, resulting in more harmful pores generated in AAC, which would cause stress concentration under load and reduce the mechanical properties of the specimen.

Fracture toughness and fracture energy. The fracture performance is crucial for brittle materials in evaluating crack development and damage evolution. Xu[7] proposed a Double K fracture model, which introduced two parameters, fracture toughness and unstable fracture toughness, to describe the initiation state and critical instability state of cracks, respectively, which can describes the ability of concrete to prevent crack propagation and is a key parameter for assessing the fracture performance of concrete.

Refer to literature [6-7], the initiation toughness and instability toughness can be calculated as following formula.

Initiation toughness K_{Ic}^{ini} :

$$K_{Ic}^{ini} = \frac{3P_{ini}S}{2BH^2}\sqrt{a_0}f(\alpha_1) \quad (1)$$

where, $f(\alpha)$ is intensity factor and can be calculated by formula (2) ~ (4). $\alpha_1 = a_0/H$. The values of a_0, and B, H, S were shown in Fig. 1.

$$f(\alpha) = \frac{\alpha^{1/2}}{(1-\alpha)^{3/2}(1+3\alpha)}\left\{p_\infty(\alpha) + \frac{4}{\beta}[p_4(\alpha) - p_\infty(\alpha)]\right\} \quad (2)$$

$$p_4(\alpha) = 1.9 + 0.41\alpha + 0.51\alpha^2 - 0.17\alpha^3 \quad (3)$$

$$p_\infty(\alpha) = 1.99 + 0.83\alpha - 0.31\alpha^2 + 0.14\alpha^3 \quad (4)$$

where, $\beta = S/H$.

Instability toughness K_{Ic}^{un} :

$$K_{Ic}^{un} = \frac{3P_{max}S}{2BH^2}\sqrt{a_c}f(\alpha_2) \quad (5)$$

where, $\alpha_2 = a_c/H$, and a_c is the length of effective crack, calculated by formula (6) ~ (11).

$$a_c = \frac{\gamma^{3/2}+m_1(\beta)\gamma}{[\gamma^2+m_2(\beta)\gamma^{3/2}+m_3(\beta)\gamma+m_4(\beta)]^{3/4}}H \quad (6)$$

$$m_1(\beta) = \beta(0.25 - 0.0505\beta^{1/2} + 0.0033\beta) \quad (7)$$

$$m_2(\beta) = \beta^{1/2}(1.155 + 0.215\beta^{1/2} - 0.278\beta) \quad (7)$$

$$m_3(\beta) =- 1.38 + 1.75\beta \quad (8)$$

$$m_4(\beta) = 0.506 - 1.057\beta + 0.888\beta^2 \quad (9)$$

$$\gamma = \frac{\omega_c BE}{6P_{max}} \quad (10)$$

$$E = \frac{1}{Bc_i}[3.70 + 32.6tan^2(\frac{\pi}{2}\cdot\frac{a_0}{H})] \quad (11)$$

where, ω_c is $COMD$ value corresponds to P_{max}. c_i is the average value of the ratio of $COMD$ value to the corresponding P at any three points during the elastic stage of the $P - COMD$ curve.

Refer to literature [8], the fracture energy can be calculated as following formula.

$$G_f = \frac{0.75W_0+W_1}{(H-a_0)B} \quad (12)$$

$$W_1 = 0.75(M_1S/L + 2M_2)\cdot g\cdot \omega_c \quad (13)$$

where, $\boldsymbol{W_0}$ is the area of $\boldsymbol{P-COMD}$ curve. $\boldsymbol{W_1}$ is the work generated by the specimen weight ($\boldsymbol{M_1}$, the values of specimens from AAC to BF/AAC-0.4 are 2.564kg, 2.614kg, 2.666kg, 2.711kg, 2.736kg, and 2.773kg, respectively) and the weight of the fixture attached to the testing machine ($\boldsymbol{M_2 = 0.82kg}$). $\boldsymbol{g}$ is 9.81m/s^2.

The fracture performance of BF/AAC with different BF content were shown in Table 2. When the BF content increased from 0.1% to 0.5%, the K_{ini} of BFAAC increased by 8.3%, 18.91%, 30.17%, 43.34% and 33.99%, respectively, the K_{Ic}^{un} increased by 20.75%, 34.6%, 66.4%, 86.66%, 87.51%, respectively, and the corresponding fracture energy increased by 18.73%, 53.38%, 83.24%, 117.75%, and 94.08%, respectively. This indicates that the addition of BF improved the toughness of AAC, and within a reasonable fiber content range, BF can suppress the initiation of AAC cracks and improve the ultimate bearing capacity.

Table 2. K_{Ic}^{ini}, K_{Ic}^{un}, and $\boldsymbol{G_f}$ of BF/AAC

No.	K_{Ic}^{ini} (Pa·m$^{1/2}$)	K_{Ic}^{un} (Pa·m$^{1/2}$)	$\boldsymbol{G_f}$ (N·m^{-1})
AAC	36.39	43.09	7.10
BF/AAC-0.1	39.41	52.03	8.43
BF/AAC-0.2	43.27	58.00	10.89
BF/AAC-0.3	47.37	71.70	13.01
BF/AAC-0.4	52.16	80.43	15.46
BF/AAC-0.5	48.76	80.80	13.78

4 Conclusions

To improve the crack resistance of AAC, BF/AAC specimens with different BF content were prepared and the corresponding fracture performance were tested. The K_{Ic}^{ini}, K_{Ic}^{un}, and $\boldsymbol{G_f}$ of BFAAC were calculated according to the double-K fracture model. In addition, SEM test was conducted to observed the microscopic morphology of BF/AAC sample. The following conclusion can be drawn.

(1) When BF content was 0.4%, the fracture performance of BF/AAC was optimal. Compared to AAC specimens without fibers, the initiation toughness, instability toughness, and fracture energy of BF/AAC-0.4% improved by 43.34%, 86.66%, and 117.75%, respectively.

(2) The adhesion between BF and pore wall matrix was good, therefore, BF deformed or was pulled out of pore wall matrix when the specimens bear external load, which consumed some energy and slightly deflected the crack propagation path on the fracture surface of AAC specimens and improved their fracture performance.

However, this study only analyzed the influence of BF content on the fracture parameters of AAC through experiments, and did not involve the fracture mechanism and crack model of BFAAC, which requires further research.

Acknowledgement

The work was supported in part by the Excellent Doctoral Dissertation Cultivation Foundation of Xi'an University of Architecture & Technology (2023XYBPY0010), the National Natural Science Foundation of China (51978566, 52378193).

References

1. X. Miao, W. Huang, Z. Fan, J. Zhang, P, Ge, Mechanical property test and numerical analysis of a novel precast shear wall. Engineering Structures, 300 (2024).
2. Y. Yardim, A. Waleed, M. Saleh Jaafar, S. Laseima, AAC-concrete light weight precast composite floor slab. Construction and Building Materials, 40, 405-410, (2013).
3. C. Xu, L. Chen, L. Y, Load-bearing tests and research on laminated floor slabs with autoclaved aerated concrete as the base slab. Journal of Shenyang Jianzhu University (Natural Science), 38 (2022).
4. W. Quan, W. Huang, Y. An, X, Miao, Z. Chen, The effect of natural bamboo fiber and basalt fiber on the properties of autoclaved aerated concrete. Construction and Building Materials, 377, (2023).
5. M. Li, A discussion of "Influence of fibrous additives on properties of aerated autoclaved concrete forming mixtures and strength characteristics of products" by A. Laukaitis, J. Keriené et al. [Construction and Building Materials 23 (9) (2009) 3034–3042]. Construction and Building Materials, 25, 2169-2170, 2011.
6. C. Ma, N. Feng, Research on the fracture behavior of gas concrete. Concrete, 10 (2005).
7. S. Xu, The calculation approaches of double-K fracture parameters of concrete and a possible coding standard test method for determining them. Journal of China Three Gorges University (Natural Sciences), 24 (2022).
8. J. Yue, H. Zhang, F. Tong, Experimental study on fracture mechanism of hardened 3D printed concrete. Journal of Building Structures, 43, 232-241, (2022).